ACS central science

Research Article

http://pubs.acs.org/journal/acscii

Why Do Membranes of Some Unhealthy Cells Adopt a Cubic Architecture?

Qi Xiao,[†] Zhichun Wang,[‡] Dewight Williams,[§] Pawaret Leowanawat,[†] Mihai Peterca,[†] Samuel E. Sherman,[†] Shaodong Zhang,[†] Daniel A. Hammer,[‡,∥] Paul A. Heiney,[⊥] Steven R. King,[#] David M. Markovitz,[#] Sabine André,[¶] Hans-Joachim Gabius,[¶] Michael L. Klein,[▽] and Virgil Percec*[,†]

[†]Roy & Diana Vagelos Laboratories, Department of Chemistry, University of Pennsylvania, Philadelphia, Pennsylvania 19104-6323, United States

[‡]Department of Bioengineering, University of Pennsylvania, Philadelphia, Pennsylvania 19104-6321, United States

[§]Electron Microscopy Resource Laboratory, Department of Biochemistry and Biophysics, Perelman School of Medicine, University of Pennsylvania, Philadelphia, Pennsylvania 19104-6082, United States

[∥]Department of Chemical and Biomolecular Engineering, University of Pennsylvania, Philadelphia, Pennsylvania 19104-6391, United States

[⊥]Department of Physics and Astronomy, University of Pennsylvania, Philadelphia, Pennsylvania 19104-6396, United States

[#]Division of Infectious Diseases, Department of Internal Medicine, Program in Immunology, University of Michigan, Ann Arbor, Michigan 48109, United States

[¶]Institute of Physiological Chemistry, Faculty of Veterinary Medicine, Ludwig-Maximilians-University, Veterinärstrasse 13, 80539 Munich, Germany

[▽]Institute of Computational Molecular Science, Temple University, Philadelphia, Pennsylvania 19122, United States

Supporting Information

ABSTRACT: Nonlamellar lipid arrangements, including cubosomes, appear in unhealthy cells, e.g., when they are subject to stress, starvation, or viral infection. The bioactivity of cubosomes—nanoscale particles exhibiting bicontinuous cubic structures—versus more common vesicles is an unexplored area due to lack of suitable model systems. Here, glycodendrimercubosomes (GDCs)—sugar-presenting cubosomes assembled from Janus glycodendrimers by simple injection into buffer—are proposed as mimics of biological cubic membranes. The bicontinuous cubic GDC architecture has been demonstrated by electron tomography. The stability of these GDCs in buffer enabled studies on lectin-dependent agglutination, revealing significant differences compared with the vesicular glycodendrimersome (GDS) counterpart. In particular, GDCs showed an increased activity toward concanavalin A, as well as an increased sensitivity and selectivity toward two variants of banana lectins, a wild-type and a genetically modified variant, which is not exhibited by GDSs. These results suggest that cells may adapt under unhealthy conditions by undergoing a transformation from lamellar to cubic membranes as a method of defense.

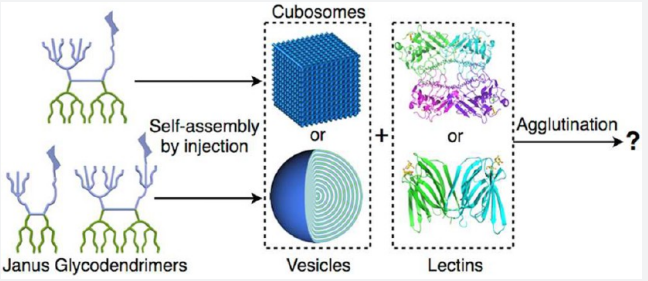

INTRODUCTION

The amphiphilic nature of phospholipids and glycolipids underlies the generation of bilayers, the biochemical platform for membranes. Physicochemical exploration of phase diagrams of lipids in water, as well as the electron tomographical monitoring of biomembranes, has unveiled an unexpected dynamic diversity of structural organization. Changes in the lipid/protein inventory of cells—artificially engineered, associated with hunger,[1] or stress induced,[2,3] for instance, in the course of viral infection[4]—can cause conversion to these unusual spatial arrangements, specifically from lamellar bilayers to bicontinuous cubic lipid phases, referred to as cubic membranes. Of note, weak intermolecular interactions between distinct epitopes of biomembranes such as cytochrome b_5 or microsomal aldehyde dehydrogenase appear as a driving force toward appearance of these nanoperiodic structures.[5,6] Cubic membranes were also proposed as an RNA antioxidant defense system, which may promote protein synthesis.[7] When prepared as tools, cubic membranes have been found to facilitate crystallization of membrane (glyco)proteins and to exhibit functional properties as transport and targeting vehicles.[8] These cell biology studies and arising practical applications prompted us to study the chemical parameters that led to the preparation

Received: September 23, 2016
Published: December 5, 2016

DOI: 10.1021/acscentsci.6b00284
ACS Cent. Sci. 2016, 2, 943−953

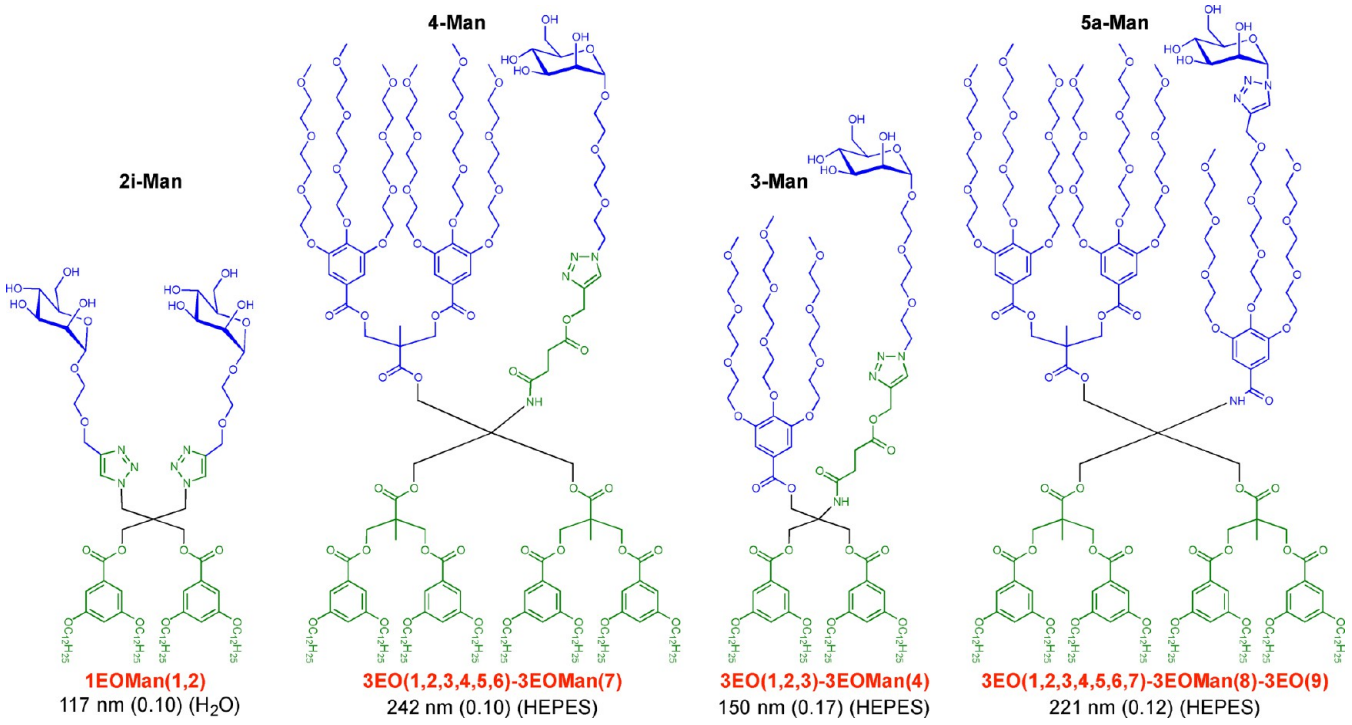

Figure 1. Molecular structures of amphiphilic Man-presenting Janus GDs. **2i-Man** [1EOMan(1,2)], **4-Man** [3EO(1,2,3,4,5,6)-3EOMan(7)], **3-Man** [3EO(1,2,3)-3EOMan(4)], and **5a-Man** [3EO(1,2,3,4,5,6,7)-3EOMan(8)-3EO(9)].[35,36,38] Solutions in THF were injected into water or HEPES buffer to give a final concentration of 0.1 mM of Man. Diameter (D_{DLS}, in nm) and polydispersity (PDI, in parentheses) were measured by dynamic light scattering (DLS).

of this phase and of the bicontinuous cubic membrane known as cubosomes.

Self-assembling block copolymers,[9−11] dendrimers,[12−14] and other building blocks[15] give rise to bicontinuous cubic phases in bulk. In aqueous phase, synthetic lipids based on monoolein[16−20] and amphiphilic block copolymers[21] spontaneously form nanoparticles denoted cubosomes[19,22−24] with $Ia\bar{3}d$ (gyroid, G surface),[19,21] $Pn\bar{3}m$ (double diamond, D surface),[19,21] or $Im\bar{3}m$ (primitive, P surface)[20,21] space group symmetry, determined by small-angle X-ray scattering (SAXS) and transmission electron microscopy (TEM).[22,25] Cubosomes assembled from lipids or block copolymers can be prepared by several methods including shaking,[19] sonication,[26] high-pressure homogenization,[27] emulsification,[28] spray drying,[29] dilution of ethanol solution with water,[22] and cosolvent dialysis.[21] Our laboratory discovered that fast injection of a solution of amphiphilic Janus dendrimers from a water-miscible solvent such as ethanol or tetrahydrofuran (THF) into aqueous media (water or buffer) followed by vortexing can form complex architectures including monodisperse vesicles, discs, tubes, fibers, and cubosomes.[30] Because of the applications of cubosomes in cosmetics,[23] protein and drug delivery,[31,32] for coassembly with membrane channel proteins,[33] and for the conjugation of bioactive molecules,[34] the simple injection method is valuable since it can prepare cubosomes in just a few seconds as compared with previous time-consuming methods. It is possible to perform systematic delineation of structure (building block)−structure (cubosome) relationships and to perform functional analysis of the topological presentation of surface-accessible groups in cubosomes, which can be compared to lamellar designs. Because of the ubiquitous presence and increasingly emerging biorelevance of carbohydrates, here we focus on a carbohydrate as the bioactive headgroup by letting glycolipid-mimicking Janus glycodendrimers (GDs) self-assemble.[35−39] The vesicular assemblies from Janus dendrimers and Janus GDs, denoted dendrimersomes and glycodendrimersomes (GDSs), respectively, demonstrated thickness,[30,40,41] permeability,[30,39] mechanical properties and stability[30] as well as encapsulating capability[30,39] comparable to biological membranes. With these biomimetic models, recent studies have gained new insight into functional aspects of natural variants of human adhesion/growth-regulatory galectins by using GDSs with varying glycan density, emphasizing the significance of glycan topology on cell membranes for lectin reactivity.[35−37,42,43] The related thickness and biocompatibility of dendrimersomes and GDSs with biological membranes facilitated their hybrid coassembly with cell membranes.[39] In fact, glycans and their lipid anchors have enormous potential for self-interaction and structural organization of domains with (glyco)proteins, as well as the capacity for serving as (patho)physiological counterreceptors for tissue receptors (lectins).[44]

The first GDCs prepared had $Pn\bar{3}m$ cubic symmetry and were stable in water but not in buffer.[35] Lack of stability in buffer prevented the use of these initial GDCs in biological testing. In the course of studying the diversity of nanoparticle populations established from a library of sequence-defined Janus GDs, the presence of GDCs in buffer was observed in addition to unilamellar and onion-like multilamellar GDSs.[38] Because the sugar D-mannose (Man) used in these initial studies is a signal in cell−cell/matrix interactions and routing of glycoproteins[44] and its presentation on GDSs[35,36,38] had been shown to maintain reactivity with the plant lectin concanavalin A (ConA), the biomedical relevance of GDCs called for their thorough structural characterization and a comparative analysis of the engagement of different types of nanoparticles including

DOI: 10.1021/acscentsci.6b00284
ACS Cent. Sci. 2016, 2, 943−953

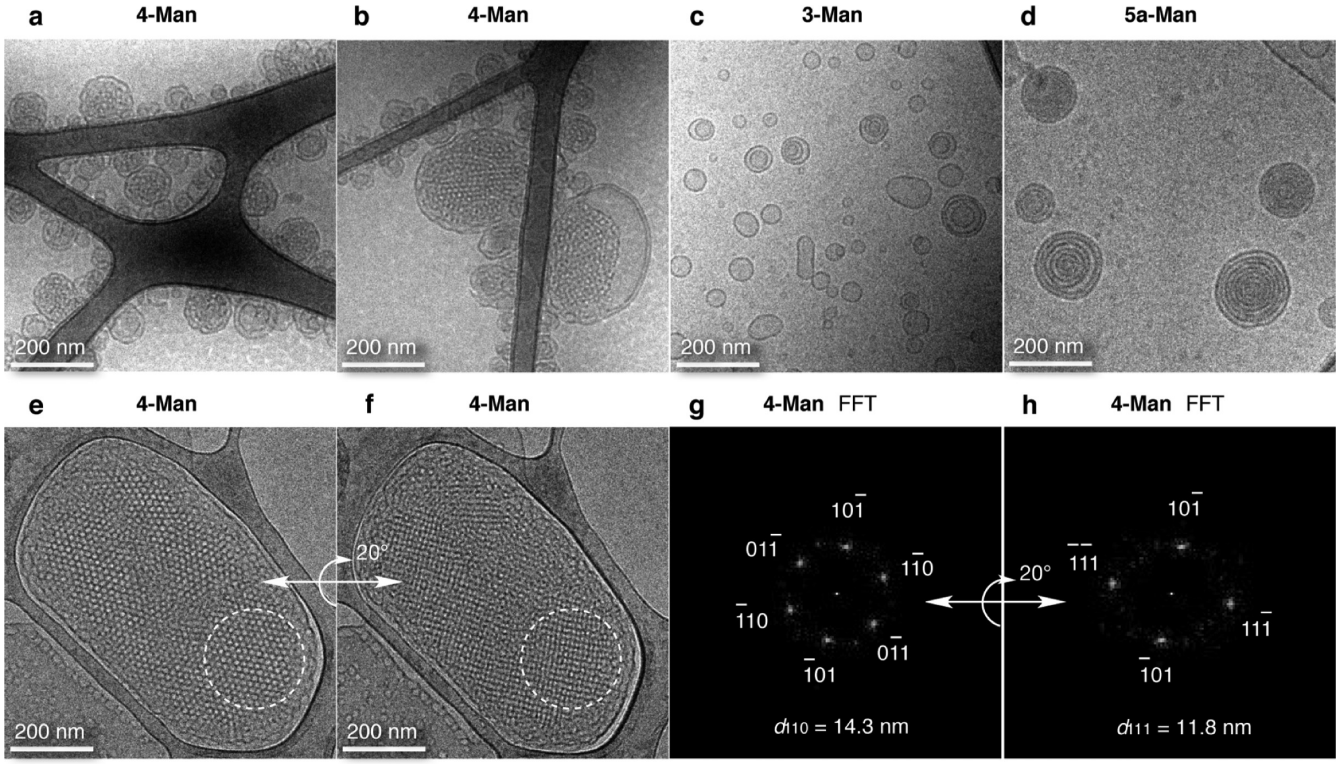

Figure 2. Cryo-TEM. (a–d) Representative cryo-TEM images of GDCs self-assembled from 0.1 mM of (a, b) **4-Man**, and onion-like GDSs self-assembled from 0.1 mM of (c) **3-Man** and (d) **5a-Man**. (e, f) Cryo-TEM images of a large particle prepared from 0.2 mM of **4-Man** imaged with (e) 0° tilt and (f) 20° tilt. (g, h) The diffraction patterns of the fast Fourier transform (FFT) patterns of the regions denoted by a broken circle in (e) and (f), respectively. The {110} and {111} features indicated arrangement in a $Pn\bar{3}m$ bicontinuous cubic phase, with a lattice parameter a of 20.3 nm surrounded by a bilayer membrane.

GDCs in lectin-dependent aggregate formation. In order to investigate variations in reactivity, two families of Man-specific lectins differing in folding and arrangement of contact sites were tested: (i) ConA[45] with β-sandwich folding, which is also common for intracellular lectins and adhesion/growth-regulatory galectins, and two sets of bivalency on opposing sides, as used previously[35,36,38] and (ii) banana lectin (BanLec) with β-prism I folding and two neighboring contact sites per subunit in the dimer.[46−49] The importance of multivalent interactions and cis-cross-linking, present in BanLec,[48,49] on the ability of lectins to yield stable aggregates with GDCs and GDSs was probed with the H84T variant of BanLec, in which these properties are diminished, causing a reduced extent of mitogenicity. Understanding lectin-dependent GDC/GDS agglutination can also be a starting point to exploit Man residues to direct multicompartmental nanocarriers such as GDCs and GDSs to specific cells, including dendritic or Langerhans cells and macrophages, by presenting a glycan tailored to the characteristic topology of their surface lectins and contact sites.[44] Binding of glycans with lectins is involved in a diversity of biologically relevant events including cell adhesion, differentiation, inflammation, proliferation, immune response such as recognition and interactions with viruses and pathogens, and growth regulation.[50−53] The newly available GDC/GDS supply the tools to investigate the effect of the transition from lamellar to cubic membranes in biological systems on the binding of glycans with lectins. These investigations will provide insight into the biological rationale for this architectural transformation as a regulatory switch for lectin−glycan interaction.

RESULTS AND DISCUSSION

Morphological Analysis of GDCs. An essential prerequisite for biorelevance is GDC stability in buffer. Initially, GDC generation had been reported after self-assembly of the amphiphilic Janus GD **2i-Man** [1EOMan(1,2)] (Figure 1) with stability restricted to water.[35] Sequence-defined variations of the headgroup led to the discovery of the GD **4-Man** [3EO(1,2,3,4,5,6)-3EOMan(7)] (Figure 1) as a suitable building block for the assembly of GDCs that are stable in 4-(2-hydroxyethyl)-1-piperazineethanesulfonic acid (HEPES) buffer.[38] Seemingly subtle structural alterations, shown for the Janus GDs **3-Man** [3EO(1,2,3)-3EOMan(4)] and **5a-Man** [3EO(1,2,3,4,5,6,7)-3EOMan(8)-3EO(9)] in Figure 1, resulted in the formation of unilamellar and multilamellar GDSs.[36,38]

The nanoparticles obtained by self-assembly in 0.1 mM HEPES buffer-based solutions of Janus GDs were analyzed by cryo-transmission electron microscopy (cryo-TEM) (Figure 2a–d). In contrast to the GDSs assembled from **3-Man** (Figure 2c) and **5a-Man** (Figure 2d), which are vesicles with distinct membrane bilayers as reported previously,[36,38] **4-Man** formed assemblies with complex interior networks (Figure 2a). Some products of **4-Man** self-assembly also include membrane bilayers (Figure 2b), which surround the bicontinuous cubic interior. Generated from a solution of increased concentration (0.2 mM of **4-Man** in HEPES, D_{DLS} = 303.2 nm, PDI = 0.15), the interior periodicity became more apparent, presenting a hexagonal honeycomb arrangement (Figure 2e) encapsulated in a bilayer membrane (Figure 2a,b,e,f and Figure S1a).

The large images from Figure 2e,f were selected to generate the Fourier transform, and their modulated bilayer periphery is

DOI: 10.1021/acscentsci.6b00284
ACS Cent. Sci. 2016, 2, 943−953

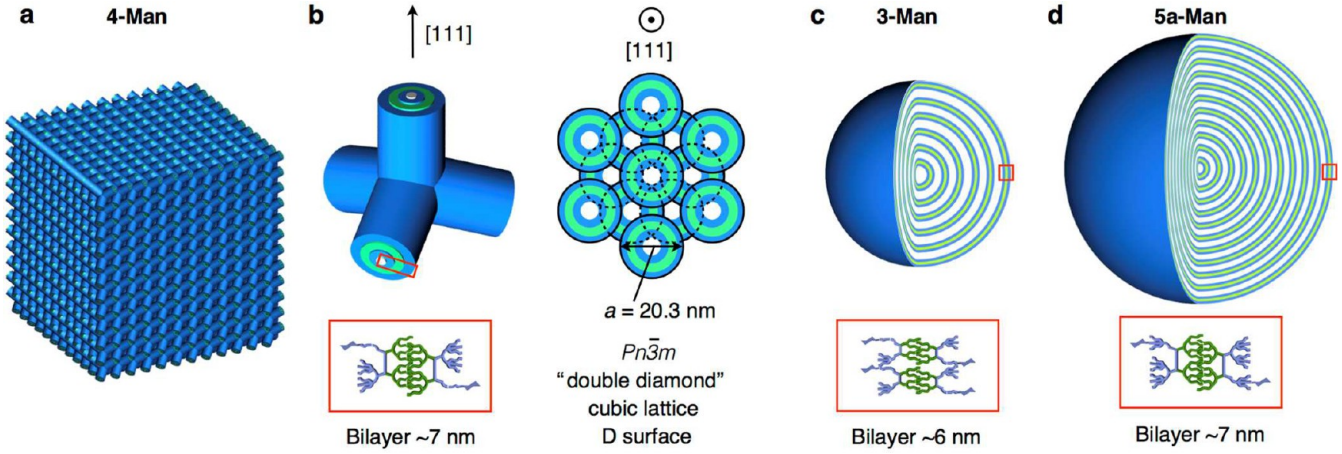

Figure 3. Supramolecular GDC models from cryo-TEM. (a) The bicontinuous cubic morphology of the interior of the GDC self-assembled from 0.1 mM of **4-Man**, and (b) a lattice unit and hexagonal arrangement of a GDC along the [111] axis, as shown in Figure 2e. (c, d) Schematic structures of the onion-like GDSs self-assembled from 0.1 mM of (c) **3-Man** and (d) **5a-Man** are presented for comparison.[38] The thicknesses of bilayers are estimated from cryo-TEM data, as described.[30,55]

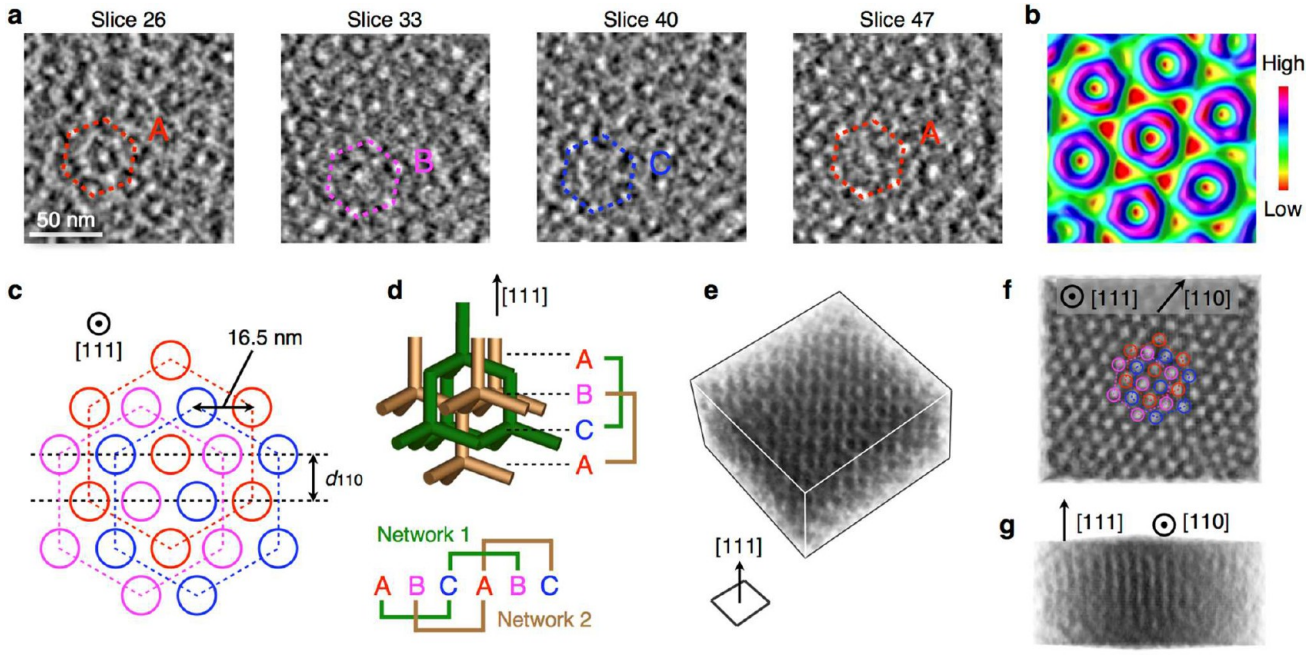

Figure 4. GDC morphology revealed in a cryo-electron tomogram. (a) Sequence of images by 3D cryo-electron tomography of GDCs assembled by **4-Man** along the [111] direction. (b) Representative electron density map from slice 26 as shown in (a). (c) Schematic representation of bicontinuous channels in the cubic phase. Red, magenta, and blue hexagons represent different layers A, B, and C, as observed in (a). (d) Schematic representation of two independent networks of water channels (network 1 in green and network 2 in brown) connected in different layers. (e, f, g) Model of the cubic phase reconstructed from 3D cryo-electron tomogram (Movies S1 and S2) presenting views from different angles, including (e) perspective view, (f) top view with overlaid pattern as shown in (c), and (g) side view.

affected by the lacey carbon of the TEM grid. Tilting this particle by 20° transformed the pattern to the arrangement as observed in studies on lipid cubosomes (Figure 2f).[25] Fast Fourier transform (FFT) analysis of selected regions was thus consistent with the $Pn\bar{3}m$ space group (double diamond, D surface). The other bicontinuous cubic phases including $Im\bar{3}m$ and $Ia\bar{3}d$, as well as the reversed micellar cubic phase $Fd\bar{3}m$, could be eliminated by their patterns at a 20° tilt, which are inconsistent with the observed pattern.[54] On the basis of the FFT patterns, d_{110} = 14.3 nm and d_{111} = 11.8 nm fit the ratio of cubic symmetric Miller indices.

$$d_{hkl} = \frac{a}{\sqrt{h^2 + k^2 + l^2}}$$

$$d_{110}: d_{111} = \frac{1}{\sqrt{2}}: \frac{1}{\sqrt{3}} \approx 1.22$$

The lattice parameter, $a = \sqrt{2} \times d_{110} = \sqrt{3} \times d_{111}$, of the $Pn\bar{3}m$ cubic lattice was calculated to be 20.3 nm, and the assemblies aligned their [111] direction perpendicular to the electron beam direction. The diffraction patterns obtained from FFT analysis of cryo-TEM enabled modeling of the GDC (Figure 3; for comparison, the GDS models in the cases of **3-Man**/**5a-Man** are also presented).[38] The thickness of a Janus

DOI: 10.1021/acscentsci.6b00284
ACS Cent. Sci. 2016, 2, 943−953

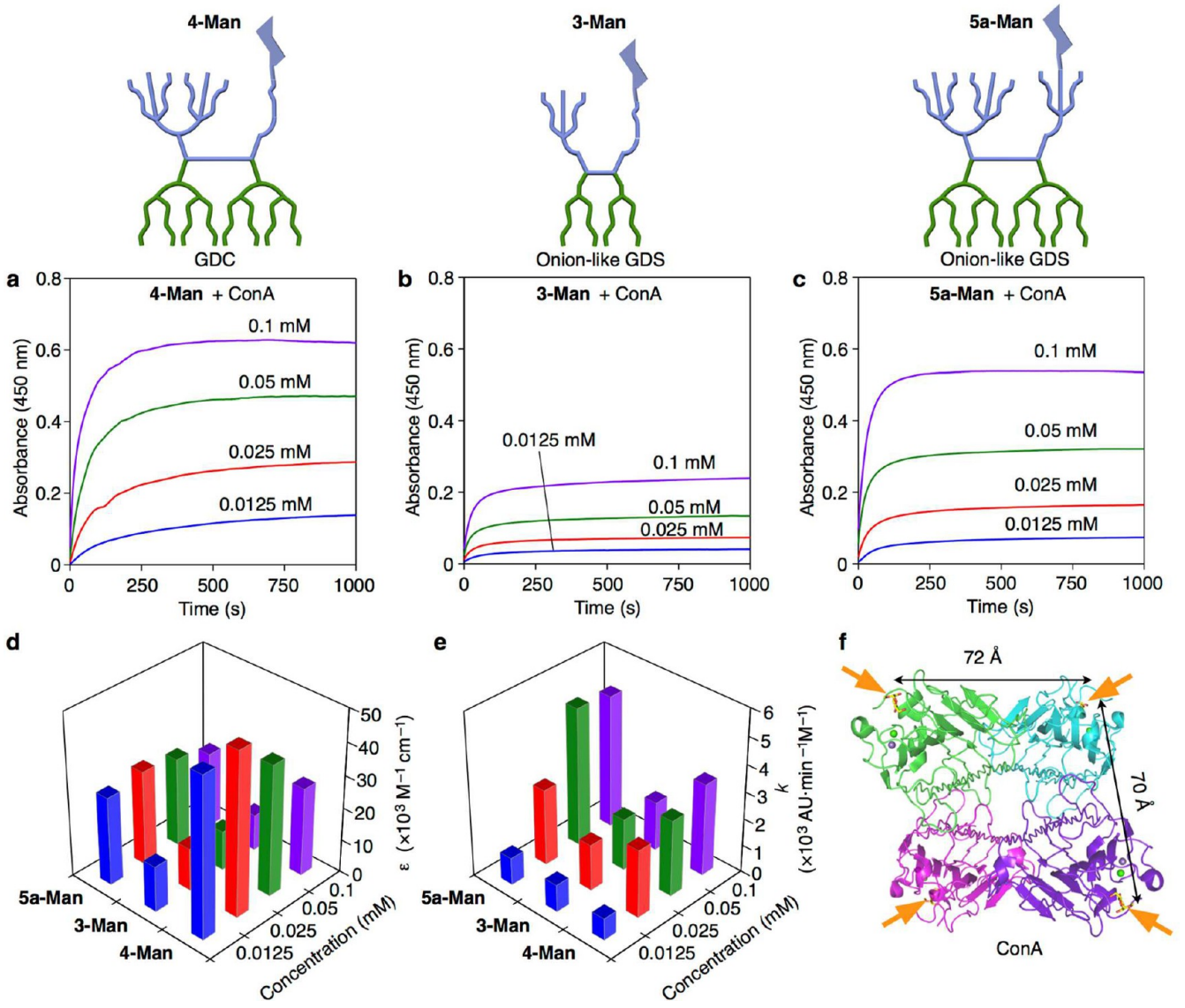

Figure 5. Agglutination assays with ConA. (a–c) Change of turbidity over time in solutions of Man-presenting GDCs self-assembled from (a) **4-Man** (0.0125–0.1 mM in 900 μL of 10 mM HEPES, 1.0 mM $CaCl_2$, and 1.0 mM $MnCl_2$), and Man-presenting onion-like GDSs self-assembled from (b) **3-Man** and (c) **5a-Man** (0.0125–0.1 mM in 900 μL of 10 mM HEPES, 1.0 mM $CaCl_2$ and 1.0 mM $MnCl_2$) with ConA (0.5 mg·mL^{-1} in 100 μL of 10 mM HEPES, 1.0 mM $CaCl_2$, and 1.0 mM $MnCl_2$). (d) Molar attenuation coefficient, ε, and (e) rate constant of change in turbidity, k, of **4-Man**, **3-Man**, and **5a-Man** with ConA. ε, is adapted from the Beer–Lambert law, $\varepsilon = A\cdot(cl)^{-1}$, where A = plateau value of absorbance, c = molar concentration of Man, and l = semimicro cuvette path length (0.23 cm). k is calculated from the curves in (a–c) in HEPES at $t_{1/2}$, where $t_{1/2}$ is the time at which the observed absorbance is equal to half of the plateau absorbance. (f) Representative illustration of the tetrameric lectin ConA, in which each binding site is loaded with the ligand methyl α-D-mannopyranoside (PDB 5CNA). The two cations Ca^{2+} (green sphere) and Mn^{2+} (purple sphere) that are essential for lectin activity are also highlighted. Orange arrows indicate Man-binding sites. The distances between binding sites are indicated.

GD bilayer and the symmetry of the $Pn\bar{3}m$ lattice require that the GDC must be constructed from cubic membranes with tetrahedral water channels (Figure 3b). Along the [111] direction, different channels in different layers overlapped (Figure 3b), calling for further analysis of the cubic structure.

Cryo-Electron Tomography (CET) and Structural Reconstruction of GDCs. The success of CET in observing the water and lipid (monoolein) network of the bicontinuous phases for cubic membrane structures of "primitive" $Im\bar{3}m$ symmetry[56] informed its use for characterizing the "double diamond" $Pn\bar{3}m$ cubosome. To reconstruct the 3D organization of $Pn\bar{3}m$ GDCs assembled from 0.1 mM of **4-Man** in HEPES, the sample holder was tilted from −60° to +60° during data collection (Movie S1). One well-defined GDC was selected for 3D reconstruction. It revealed that sections along the [111] direction, which is the electron beam direction, show a hexagonal arrangement of circles, which appear periodically upon moving along the [111] direction (Movie S2). Illustrations of slices with order numbers of 26, 33, 40, and 47 are shown in Figure 4a. Hexagons referred to as A (red), B (magenta), and C (blue) define water channels in different layers of the cubosome. Electron density maps reveal the high electron density of the Janus GD bilayers and the low electron density of water channels as expected (Figure 4b). The bicontinuous cubic channels of $Pn\bar{3}m$ GDCs were well resolved when combining the A, B, and C channels (Figure 4c). Two

DOI: 10.1021/acscentsci.6b00284
ACS Cent. Sci. 2016, 2, 943–953

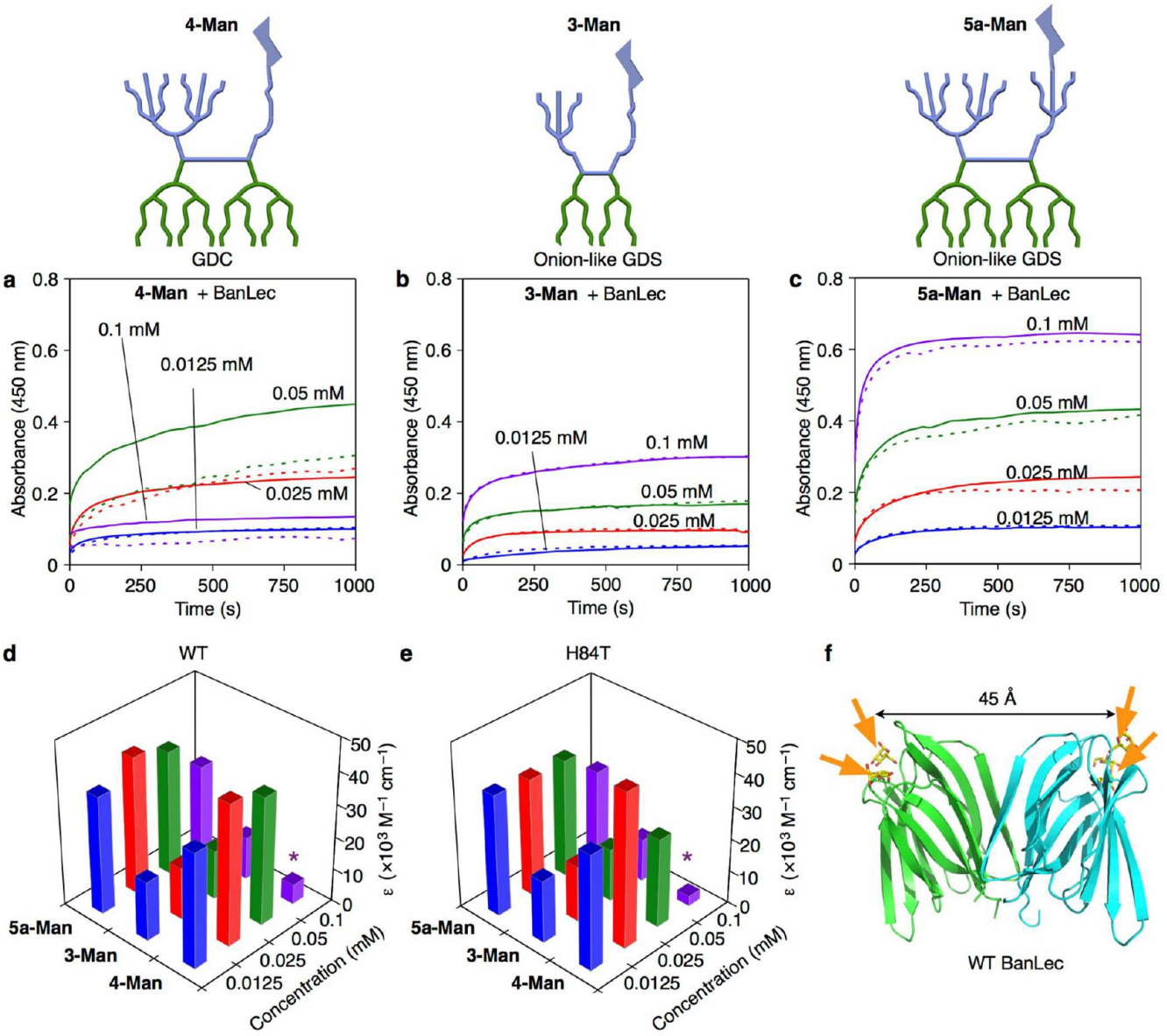

Figure 6. Agglutination assays with WT BanLec and its H84T variant. (a–c) Agglutination assays of Man-presenting GDCs self-assembled from (a) **4-Man** (0.0125–0.1 mM in 900 μL of 10 mM HEPES), and Man-presenting onion-like GDSs self-assembled from (b) **3-Man** and (c) **5a-Man** (0.0125–0.1 mM in 900 μL of 10 mM HEPES) with WT BanLec (solid lines) and its H84T variant (broken lines) (0.5 mg·mL^{-1} in 100 μL of 10 mM HEPES). (d, e) Molar attenuation coefficient, ε of **4-Man**, **3-Man**, and **5a-Man** with (d) WT BanLec or (e) its variant. ε is adapted from the Beer–Lambert law, $\varepsilon = A\cdot(cl)^{-1}$, where A = plateau value of absorbance, c = molar concentration of Man, and l = semimicro cuvette path length (0.23 cm). (f) Crystallographic structure of the dimeric WT BanLec loaded with dimannose (PDB 4PIK). Orange arrows indicate Man-binding sites. Distance between binding sites is indicated.

sets of independent networks are shown in Figure 4d, with network 1 (green) connecting nonadjacent A–C–B channel layers and network 2 (brown) nonadjacent B–A–C channel layers. A model of the cubic phase in the GDC (Figure 4e–g) reconstructed from CET (Movie S2) illustrates the hexagonal arrangement of channels (Figure 4f). In particular, A, B, and C channels can be observed, suggesting that the supramolecular model presented in Figure 3a,b is consistent with experimental cryo-TEM data (Figure 2e). Although the exact morphology of the outer membrane of the GDCs has not been elucidated,[56] it is apparent from cryo-TEM that its topology is modulated by the internal cubic morphology generating an undulating contour of the surface with variable curvature (Figure S1a, Movies S1 and S2). Therefore, the topology of the outer membrane of the GDC appears to be strongly influenced by its interior structure.[22,26,56] The morphology of the outer membrane of the GDCs thus appears to be fundamentally different from the smooth and nearly uniform curvature of the membranes of GDSs (Figure 2c–d) which are not influenced by their interior structure. As a means of investigating the influence of these different outer-membrane morphologies on function in a biological context, lectin reactivity of the GDCs could be directly compared to the reactivity of GDSs.

Lectin-Dependent GDC/GDS Agglutination. The turbidity increase after addition of lectin into buffer containing GDC/GDS is due to carbohydrate-dependent agglutination, which has been visualized with cryo-TEM in Figure S1b for GDC and reported previously for GDS.[35,42] Its monitoring with

DOI: 10.1021/acscentsci.6b00284
ACS Cent. Sci. 2016, 2, 943–953

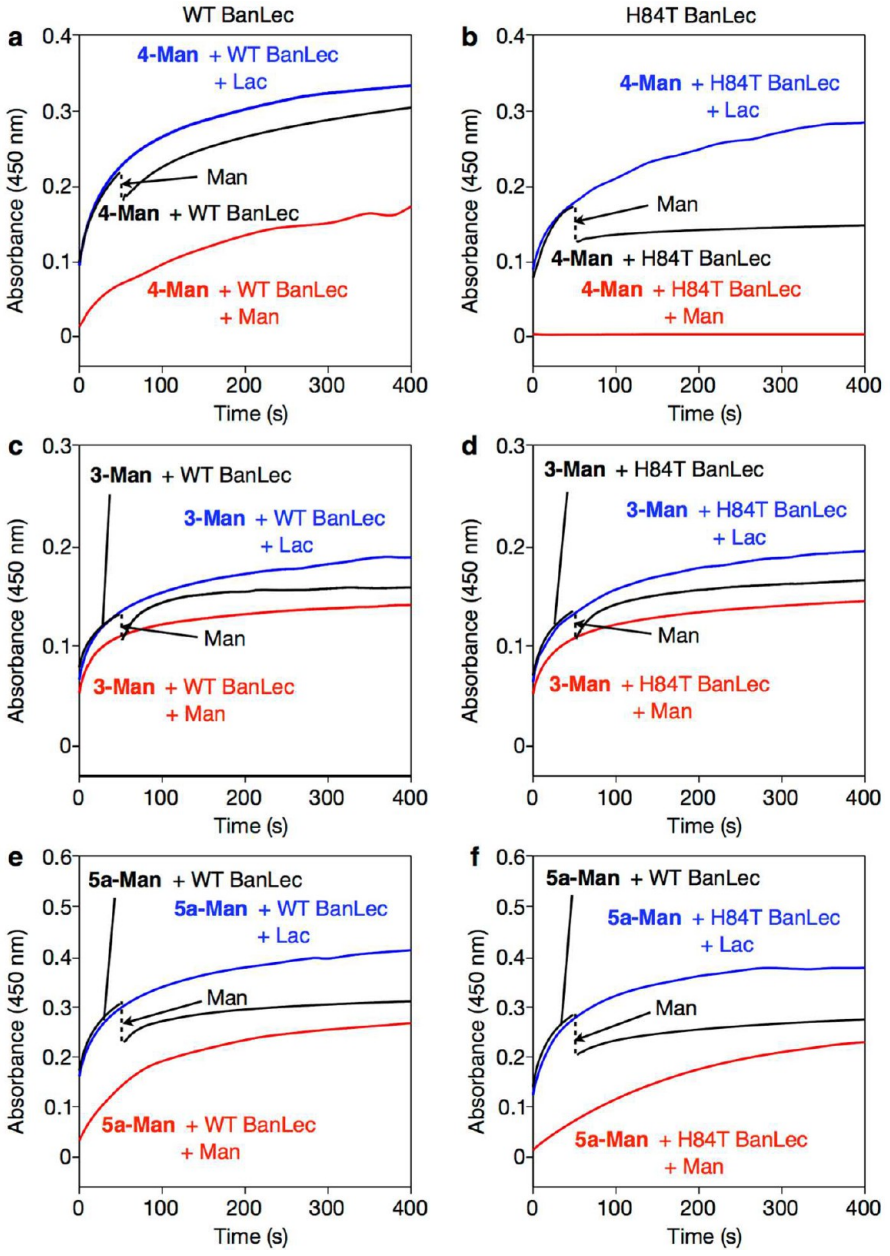

Figure 7. Agglutination assays with WT BanLec and its H84T variant. Man-presenting (a–b) GDCs self-assembled from **4-Man**, and onion-like GDSs self-assembled from (c–d) **3-Man** and (e–f) **5a-Man**, prepared with 0.05 mM of Janus GDs, 900 μL of HEPES were incubated with WT BanLec (a, c, e) or in H84T variant (b, d, f) (0.5 mg·mL^{-1} in 100 μL of HEPES) with 100 mM of Man (red line) or Lac (blue line). A high concentration (100 mM) of Man solution in HEPES (100 μL) was added at t = 50 s into GDCs or onion-like GDSs (900 μL of HEPES) with WT BanLec (a, c, e) or H84T (b, d, f) (black line).

UV–vis provides a measure of the plateau level for particle agglutination and the slope of the curve provides a measure of the rate.[35−38,42,43,57] The size of the GDCs increased from 115 to 242 nm with increase of Janus GD concentration (Figure S2).

As illustrated by the respective curves and data obtained from incubating ConA with GDC/GDS at increasing concentrations of Man (Figure 5 and Figure S3), GDCs were most reactive, extending initial data.[38] Although the GDCs were most reactive toward ConA (Figure 5d), they exhibited a reduced rate of agglutination as compared to the onion-like GDSs derived from **5a-Man** (Figure 5e), indicating differences in glycan architecture. On the other hand, both GDSs (**5a-Man** and **3-Man**) show similar correlations between reactivity and rate, reflecting their similar onion-like vesicular architectures (Figure 5d–e). The reduced rate observed for GDCs is unique as compared to all previous studies on GDSs self-assembled from Man and lactose (Lac) presenting sequence-defined GDs, which consistently exhibit an increased rate corresponding with an increase in reactivity.[37,38] In contrast to the **5a-Man**-derived GDSs,[38] aggregates of GDCs with ConA maintain some stability even after addition of cognate sugar (Figure S4). Saturating ConA with sugar by coincubation with the cognate sugar Man (but not a noncognate sugar, i.e., Lac) blocked particle agglutination nearly completely, serving as a specificity control (Figure S4). To check for carbohydrate-independent aggregation, a β-sandwich protein with reactivity toward Lac, human galectin-3 (Gal-3) was added into Man-presenting

DOI: 10.1021/acscentsci.6b00284
ACS Cent. Sci. 2016, 2, 943–953

GDCs/GDSs as a control experiment (Figure S5−S6). No measurable agglutination was observed over a period of 1000 s. Because the extent and rate of agglutination by trans-interactions critically depend on the interplay of topological features on both GDC and lectin, it is essential to pursue further testing by altering lectin properties, thus taking into account the vital aspect of multivalent contacts.

BanLec is another Man-specific lectin that is known to inhibit viruses such as HIV and influenza A.[48,49] The dimeric β-prism I lectin BanLec differs in the positioning and distance of the four Man-binding sites (Figure 6f and Figure S7) from tetrameric ConA (Figure 5f). Although the topological pattern of contact points for BanLec between particles is different from that of ConA, it, too, is a potent hemagglutinin.[48] A modified version of the wild-type (WT) BanLec, in which histidine 84 is replaced with a threonine residue (H84T), exhibits reduced activity at one binding site while preserving activity at the other binding site (Figure S7b). The H84T variant showed lower multivalent activity but retained monovalent activity and antiviral potency.[48] Until this study, neither BanLec had been used in agglutination experiments with a suitable model of a biological membrane.

At low GD concentrations, the profiles of GDC/GDS agglutination by both WT and H84T BanLec resembled that for ConA (Figures 5 and 6). However, at 0.1 mM a marked decrease in change of turbidity was measured for GDCs (purple asterisks in Figure 6d−e and Figure S8). A more detailed investigation between 0.05 and 0.1 mM revealed a maximum response to BanLec at about 0.07 mM (Figure S9). Thus, GDCs were less susceptible to agglutination with this dimeric lectin than with tetrameric ConA beyond a threshold concentration, distinguishing GDCs and GDSs on the basis of agglutination. The drastically reduced responsiveness of GDCs at 0.1 mM for BanLec illustrated the utmost importance of the topological mode of contact-site presentation by the lectin, a source of selectivity when considering biomedical applications. In physiological terms, a transition to the cubic phase may thus act as a switch for reactivity with a distinct tissue lectin such as an adhesion/growth-regulatory galectin, highlighting the possibility for differential functional pairing. Of note, BanLec's engineered variant already showed this deviation at 0.05 mM (Figure 6 and Figure S8).

The stability and reversibility of agglutination were tested for BanLec as for ConA by addition of Man. For GDSs, both BanLec variants provided identical binding curves (Figure 7c−d and Figure 7e−f). The inhibition of agglutination with BanLec was weaker than with ConA, as indicated by the increase in absorbance observed even after addition of a large amount of Man. For GDCs from **4-Man**, agglutination with WT and H84T BanLec exhibited different responses in the presence of Man. The H84T variant is significantly inhibited by Man. No agglutination was observed when Man was added to the GDC solution before addition of H84T BanLec (Figure 7b, red curve). Similarly, the agglutination progress almost stopped upon addition of Man 50 s after agglutination started with the H84T variant (Figure 7b, black curve). By comparison, aggregation of GDCs with WT BanLec (Figure 7a) was evident even in the presence of Man. These sets of experiments with two variants of BanLec demonstrate a substantial difference in the interactions of GDCs and GDSs with BanLec WT and H84T.

The similarity in the trends observed for GDSs despite the differences in chemical structures of their constituent molecules reported here for **5a-Man** and **3-Man** (Figure 6b,c) and in other publications[35,36] indicates that morphology rather than chemical structure alone appears to be the driving force behind variation in lectin reactivity. Furthermore, previous studies on GDSs with WT and mutated galectin-8 variants[43] demonstrated the activity is not determined by the chemical structures of Janus dendrimers but rather by the nature of galectins. For WT and H84T BanLec here, H84T is expected to be less active than WT BanLec,[48] but only GDCs can discriminate between the two. Thus, the different trend observed for GDCs is most likely attributable to the membrane morphology rather than the chemical structure of **4-Man**. Because of the limited stability of some of the GDS and GDC, three series of experiments with WT and H84T BanLec lectins were carried out in water rather than in buffer in order to support this morphology trend. The first series refers to identical GDS morphology with different chemistries on the periphery (**2-Man** [3EOMan(1,2)],[38] **3-Man**, and **5a-Man**, Figure S10); the second series refers to different morphologies with different chemistries on the periphery (**4-Man** displaying GDC and **5a-Man** displaying GDS, Figure S10); the third series refers to almost identical chemistries but different morphologies (**2-Man** forming GDS and **2i-Man** forming GDC, Figure S10). The first series of experiments demonstrated, as previously reported,[38] that dilution of Man via a sequence-defined methodology increases both reactivity and selectivity (Figure S10). The second series of experiments demonstrated increased reactivity and selectivity by decreased Man concentration (Figure S10). The third series of experiments demonstrated that almost identical chemistries, differing only in the number of ethylene glycol units from the spacer of the Janus glycodendrimer, provided for different morphologies different rates and different reactivity (Figure S10). Stability experiments reported for this series (compare Figures S10 and S11) support this conclusion. Therefore, while the first two series of experiments demonstrated that it is difficult to disentangle chemistry from morphology, the third series of experiments demonstrated that for almost similar chemistries the morphology determines the reactivity, the rate, and the stability.

Recent work demonstrated that a cytokine receptor mutant, which exhibited an additional glycosylation site, showed greater reactivity toward lectins, resulting in its post-lectin-binding partitioning into a nanodomain that prevented proper functioning.[58] Likewise, changes in membrane morphology via a switch from lamellar to cubic architecture may be an alternative route, distinct from mutation, through which the functionality of a receptor may be enhanced or impaired by altering the reactivity of the receptor toward lectins via a topological change in sugar presentation, rather than a gain or loss of a glycosylation site. In addition, the cytokine receptor in the previous study plays an essential role in defense against bacterial infection,[58] indicating that changes in membrane morphology may be pertinent as a regulatory switch for controlling the function of membrane proteins involved in cell defense by altering their reactivity toward lectins and thus their partitioning into nanodomains.

These studies of GDCs and GDSs with lectins such as ConA and BanLec reveal differences in bioactivity of cubic membranes and lamellar membranes and therefore provide insight into the conversion of lamellar biological membranes to cubic membranes[59] under unhealthy conditions.

DOI: 10.1021/acscentsci.6b00284
ACS Cent. Sci. 2016, 2, 943−953

CONCLUSION

The preparation of GDCs, showing a $Pn\bar{3}m$ structure, stable in buffer reported here, along with previously prepared GDSs stable in buffer, formed a model system for comparing the function toward sugar receptors of cubic membranes found in diseased cells to lamellar membranes in healthy cells. Agglutination experiments involving the three lectins ConA, wild-type (WT) BanLec, and genetically modified (H84T) BanLec, the latter two having never been previously employed in such experiments, were performed to investigate the difference in reactivity to sugar receptors between GDCs, as models of diseased cell membranes, and GDSs, as models of healthy cell membranes. For the agglutination with the classic tetrameric mannose-binding ConA, GDCs showed higher activity than GDSs. Agglutination with dimeric mannose-binding BanLec revealed a dramatic decrease in binding at high concentration (0.1 mM) for GDCs that did not occur for GDSs. Furthermore, GDCs showed reduced reactivity toward agglutination with H84T BanLec, as well as diminished aggregate stability, as compared to agglutination with WT BanLec. On the other hand, GDSs showed no significant difference in agglutination with WT versus H84T BanLec, indicating an inability to discriminate between the two lectins. This study demonstrates a sensitivity and selectivity of GDCs to agglutination with various lectins that are not present in GDSs, indicating that cells may thus adapt in unhealthy conditions by undergoing a transition from lamellar membranes to cubic membranes as a means of defense. Building on previous studies,[58] changes in membrane morphology, which alter sugar topology, may impact the reactivity of receptors involved in cell defense toward lectins, supplying a regulatory pathway by which the function of the receptors can be enhanced or impaired. Although this study does not provide a complete answer to *why the membranes of some unhealthy cells adopt a cubic architecture* (Figure S12), it provides the first clues to answering this unexplored question. These results encourage further exploration of GDCs and GDSs as model systems for the cell membranes in diseased and healthy cells as a method to understand the structure−disease relationship, with relevance to biomedical applications.

METHODS

Preparation of GDCs and GDSs. GDCs and GDSs were generated by fast injection of 100 μL of a solution of amphiphilic Janus GDs in distilled THF into 2.0 mL of water or HEPES buffer, immediately followed by vortexing for approximately 5 s.

Dynamic Light Scattering. DLS measurements of GDCs or GDSs were performed with a Malvern Zetasizer Nano-S instrument equipped with a 4 mW He−Ne laser (633 nm) and avalanche photodiode positioned at 175° to the beam. Instrument parameters and measurement times were determined automatically. Experiments were performed in triplicate.

Cryo-Transmission Electron Microscopy. Cryo-TEM was performed on an FEI Tecnai G2 12 microscope at voltage of 80 or 120 kV. Briefly, a droplet of 2 μL of a solution of GDS or GDC was pipetted onto a lacey carbon film coated on a copper grid loaded into a Gatan Cp3 cryoplunger. The sample was blotted by hand for ∼6 s and then quickly plunged into liquefied ethane (∼90 K) cooled by a reservoir of liquid nitrogen to ensure the vitrification of water. The vitrified samples were transferred to a Gatan 626 cryoholder in a cryo-transfer stage immersed in liquid nitrogen. During the imaging, the cryoholder was kept below −175 °C to prevent sublimation of vitreous solvent. The digital images were recorded by a Gatan low dose US1000 CCD camera. Image processing and analysis were completed with ImageJ v1.50.

Cryo-Electron Tomography. Colloidal gold was added to the sample to act as a fiducial marker for CET. To obtain a sufficient dispersion of colloidal gold, the colloidal suspension was spun down for 20 s and then resuspended into the GDC solution, which concentrated the particles 5-fold. Sample vitrification and imaging otherwise proceeded identically as described above. Single-tilt series from −60° to +60° along the alpha axis were collected by SerialEM at 1.5° increments. Sample processing was done with IMOD[60] using the eTomo interface. As a US1000 charge-coupled device camera was used, and any random outlier pixels from X-rays were removed before image processing. A coarse alignment was done with the image shift calculated from the cross-correlations, and then a fine alignment was done by minimizing residual error in the fiducial model. A boundary model using sample tomograms was used to minimize the final tomogram volume and create the full aligned stack. The final 3D reconstruction was generated using SIRT and presented by UCSF Chimera.

Lectin-Dependent Agglutination. Agglutination assays of GDCs or GDSs with lectin (ConA and BanLec) were monitored in semimicro disposable cuvettes (path length, l = 0.23 cm) at 23 °C at wavelength λ = 450 nm by using a Shimadzu UV−vis spectrophotometer UV-1601 with Shimadzu/UV Probe software in kinetic mode. HEPES solution of lectin (100 μL) was injected into HEPES solution of GDCs or GDSs (900 μL). The cuvette was shaken by hand for 1−2 s before data collection was started. The same solution of GDCs or GDSs solution was used as a reference. HEPES solutions of lectin were prepared before the agglutination assays and were maintained at 0 °C (ice bath) before data collection.

ASSOCIATED CONTENT

Supporting Information

The Supporting Information is available free of charge on the ACS Publications website at DOI: 10.1021/acscentsci.6b00284.

Supporting materials and figures (PDF)
Movies S1 (AVI1) and S2 (AVI2)

AUTHOR INFORMATION

Corresponding Author

*E-mail: percec@sas.upenn.edu.

ORCID

Qi Xiao: 0000-0002-6470-0407
Mihai Peterca: 0000-0002-7247-4008
Virgil Percec: 0000-0001-5926-0489

Notes

The authors declare the following competing financial interest(s): D.M.M. is the founder of Virule, Inc., set up to develop H84T BanLec as an antiviral agent. The other authors declare no competing financial interests.

ACKNOWLEDGMENTS

Financial support from the National Science Foundation (Grants DMR-1066116 and DMR-1120901), the P. Roy Vagelos Chair at the University of Pennsylvania, and the Humboldt Foundation (all to V.P.), National Science

DOI: 10.1021/acscentsci.6b00284
ACS Cent. Sci. 2016, 2, 943−953

Foundation (Grant DMR-1120901 to D.A.H., P.A.H., and M.L.K.), the University of Michigan MTRAC Life Sciences (to D.M.M.), the Biomolecular Materials Program at the U. S. Department of Energy, Office of Basic Energy Science, Division of Materials Science (Grant DE-SC0007063 to D.A.H.), and the EC Seventh Framework Programme (GLYCOPHARM to H.-J.G.) is gratefully acknowledged, as are inspiring discussions with Drs. B. Friday and A. Leddoz.

REFERENCES

(1) Daniels, E. W.; Breyer, E. P. Starvation effects on the ultrastructure of amoeba mitochondria. *Cell Tissue Res.* **1968**, *91*, 159−169.
(2) Almsherqi, Z. A.; Kohlwein, S. D.; Deng, Y. Cubic membranes: a legend beyond the Flatland* of cell membrane organization. *J. Cell Biol.* **2006**, *173*, 839−844.
(3) Almsherqi, Z. A.; Landh, T.; Kohlwein, S. D.; Deng, Y. Cubic membranes: the missing dimension of cell membrane organization. *Int. Rev. Cell Mol. Biol.* **2009**, *274*, 275−342.
(4) Deng, Y.; Almsherqi, Z. A.; Ng, M. M. L.; Kohlwein, S. D. Do viruses subvert cholesterol homeostasis to induce host cubic membranes? *Trends Cell Biol.* **2010**, *20*, 371−379.
(5) Yamamoto, A.; Masaki, R.; Tashiro, Y. Formation of crystalloid endoplasmic reticulum in COS cells upon overexpression of microsomal aldehyde dehydrogenase by cDNA transfection. *J. Cell Sci.* **1996**, *109*, 1727−1738.
(6) Snapp, E. L.; Hegde, R. S.; Francolini, M.; Lombardo, F.; Colombo, S.; Pedrazzini, E.; Borgese, N.; Lippincott-Schwartz, J. Formation of stacked ER cisternae by low affinity protein interactions. *J. Cell Biol.* **2003**, *163*, 257−269.
(7) Deng, Y.; Almsherqi, Z. A. Evolution of cubic membranes as antioxidant defence system. *Interface Focus* **2015**, *5*, 20150012.
(8) Caffrey, M. A comprehensive review of the lipid cubic phase or in meso method for crystallizing membrane and soluble proteins and complexes. *Acta Crystallogr., Sect. F: Struct. Biol. Commun.* **2015**, *71*, 3−18.
(9) Thomas, E. L.; Alward, D. B.; Kinning, D. J.; Martin, D. C.; Handlin, D. L.; Fetters, L. J. Ordered bicontinuous double-diamond structure of star block copolymers: a new equilibrium microdomain morphology. *Macromolecules* **1986**, *19*, 2197−2202.
(10) Hasegawa, H.; Tanaka, H.; Yamasaki, K.; Hashimoto, T. Bicontinuous microdomain morphology of block copolymers. *Macromolecules* **1987**, *20*, 1651−1662.
(11) Thomas, E. L.; Anderson, D. M.; Henkee, C. S.; Hoffman, D. Periodic area-minimizing surfaces in block copolymers. *Nature* **1988**, *334*, 598−601.
(12) Chvalun, S. N.; Shcherbina, M. A.; Yakunin, A. N.; Blackwell, J.; Percec, V. Structure of gyroid mesophase formed by monodendrons with fluorinated alkyl tails. *Polym. Sci., Ser. A* **2007**, *49*, 158−167.
(13) Rosen, B. M.; Wilson, C. J.; Wilson, D. A.; Peterca, M.; Imam, M. R.; Percec, V. Dendron-mediated self-assembly, disassembly, and self-organization of complex systems. *Chem. Rev.* **2009**, *109*, 6275−6540.
(14) Rosen, B. M.; Peterca, M.; Huang, C.; Zeng, X.; Ungar, G.; Percec, V. Deconstruction as a strategy for the design of libraries of self-assembling dendrons. *Angew. Chem., Int. Ed.* **2010**, *49*, 7002−7005.
(15) Huang, M.; Hsu, C.-H.; Wang, J.; Mei, S.; Dong, X.; Li, Y.; Li, M.; Liu, H.; Zhang, W.; Aida, T.; Zhang, W.-B.; Yue, K.; Cheng, S. Z. D. Selective assemblies of giant tetrahedra *via* precisely controlled positional interactions. *Science* **2015**, *348*, 424−428.
(16) Luzzati, V.; Husson, F. The structure of the liquid-crystalline phase of lipid-water systems. *J. Cell Biol.* **1962**, *12*, 207−219.
(17) Luzzati, V.; Tardieu, A.; Gulik-Krzywicki, T. Polymorphism of lipids. *Nature* **1968**, *217*, 1028−1030.
(18) Luzzati, V.; Tardieu, A.; Gulik-Krzywicki, T.; Rivas, E.; Reiss-Husson, F. Structure of the cubic phases of lipid−water systems. *Nature* **1968**, *220*, 485−488.
(19) Larsson, K. Cubic lipid-water phases: structures and biomembrane aspects. *J. Phys. Chem.* **1989**, *93*, 7304−7314.
(20) Landh, T. Phase behavior in the system pine needle oil monoglycerides-poloxamer 407-water at 20.degree. *J. Phys. Chem.* **1994**, *98*, 8453−8467.
(21) La, Y.; Park, C.; Shin, T. J.; Joo, S. H.; Kang, S.; Kim, K. T. Colloidal inverse bicontinuous cubic membranes of block copolymers with tunable surface functional groups. *Nat. Chem.* **2014**, *6*, 534−541.
(22) Spicer, P. T.; Hayden, K. L.; Lynch, M. L.; Ofori-Boateng, A.; Burns, J. L. Novel process for producing cubic liquid crystalline nanoparticles (cubosomes). *Langmuir* **2001**, *17*, 5748−5756.
(23) Spicer, P. Cubosome processing: industrial nanoparticle technology development. *Chem. Eng. Res. Des.* **2005**, *83*, 1283−1286.
(24) Garg, G.; Saraf, S.; Saraf, S. Cubosomes: an overview. *Biol. Pharm. Bull.* **2007**, *30*, 350−353.
(25) Sagalowicz, L.; Michel, M.; Adrian, M.; Frossard, P.; Rouvet, M.; Watzke, H. J.; Yaghmur, A.; De Campo, L.; Glatter, O.; Leser, M. E. Crystallography of dispersed liquid crystalline phases studied by cryo-transmission electron microscopy. *J. Microsc.* **2006**, *221*, 110−121.
(26) Gustafsson, J.; Ljusberg-Wahren, H.; Almgren, M.; Larsson, K. Cubic lipid−water phase dispersed into submicron particles. *Langmuir* **1996**, *12*, 4611−4613.
(27) Siekmann, B.; Bunjes, H.; Koch, M. H. J.; Westesen, K. Preparation and structural investigations of colloidal dispersions prepared from cubic monoglyceride−water phases. *Int. J. Pharm.* **2002**, *244*, 33−43.
(28) Esposito, E.; Cortesi, R.; Drechsler, M.; Paccamiccio, L.; Mariani, P.; Contado, C.; Stellin, E.; Menegatti, E.; Bonina, F.; Puglia, C. Cubosome dispersions as delivery systems for percutaneous administration of indomethacin. *Pharm. Res.* **2005**, *22*, 2163−2173.
(29) Spicer, P. T.; Small, W. B., II; Small, W. B.; Lynch, M. L.; Burns, J. L. Dry powder precursors of cubic liquid crystalline nanoparticles (cubosomes). *J. Nanopart. Res.* **2002**, *4*, 297−311.
(30) Percec, V.; Wilson, D. A.; Leowanawat, P.; Wilson, C. J.; Hughes, A. D.; Kaucher, M. S.; Hammer, D. A.; Levine, D. H.; Kim, A. J.; Bates, F. S.; Davis, K. P.; Lodge, T. P.; Klein, M. L.; DeVane, R. H.; Aqad, E.; Rosen, B. M.; Argintaru, A. O.; Sienkowska, M. J.; Rissanen, K.; Nummelin, S.; Ropponen, J. Self-assembly of Janus dendrimers into uniform dendrimersomes and other complex architectures. *Science* **2010**, *328*, 1009−1014.
(31) Angelov, B.; Angelova, A.; Filippov, S. K.; Drechsler, M.; Štěpánek, P.; Lesieur, S. Multicompartment lipid cubic nanoparticles with high protein upload: millisecond dynamics of formation. *ACS Nano* **2014**, *8*, 5216−5226.
(32) Karami, Z.; Hamidi, M. Cubosomes: remarkable drug delivery potential. *Drug Discovery Today* **2016**, *21*, 789−801.
(33) Speziale, C.; Salvati Manni, L. S.; Manatschal, C.; Landau, E. M.; Mezzenga, R. A macroscopic H^+ and Cl^- ions pump *via* reconstitution of EcClC membrane proteins in lipidic cubic mesophases. *Proc. Natl. Acad. Sci. U. S. A.* **2016**, *113*, 7491−7496.
(34) Aleandri, S.; Bandera, D.; Mezzenga, R.; Landau, E. M. Biotinylated cubosomes: a versatile tool for active targeting and codelivery of paclitaxel and a fluorescein-based lipid dye. *Langmuir* **2015**, *31*, 12770−12776.
(35) Percec, V.; Leowanawat, P.; Sun, H.-J.; Kulikov, O.; Nusbaum, C. D.; Tran, T. M.; Bertin, A.; Wilson, D. A.; Peterca, M.; Zhang, S.; Kamat, N. P.; Vargo, K.; Moock, D.; Johnston, E. D.; Hammer, D. A.; Pochan, D. J.; Chen, Y.; Chabre, Y. M.; Shiao, T. C.; Bergeron-Brlek, M.; André, S.; Roy, R.; Gabius, H.-J.; Heiney, P. A. Modular synthesis of amphiphilic Janus glycodendrimers and their self-assembly into glycodendrimersomes and other complex architectures with bioactivity to biomedically relevant lectins. *J. Am. Chem. Soc.* **2013**, *135*, 9055−9077.
(36) Zhang, S.; Moussodia, R.-O.; Sun, H.-J.; Leowanawat, P.; Muncan, A.; Nusbaum, C. D.; Chelling, K. M.; Heiney, P. A.; Klein, M. L.; André, S.; Roy, R.; Gabius, H.-J.; Percec, V. Mimicking biological membranes with programmable glycan ligands self-assembled from amphiphilic Janus glycodendrimers. *Angew. Chem., Int. Ed.* **2014**, *53*, 10899−10903.

DOI: 10.1021/acscentsci.6b00284
ACS Cent. Sci. 2016, 2, 943−953

(37) Zhang, S.; Xiao, Q.; Sherman, S. E.; Muncan, A.; Ramos Vicente, A. D. M.; Wang, Z.; Hammer, D. A.; Williams, D.; Chen, Y.; Pochan, D. J.; Vértesy, S.; André, S.; Klein, M. L.; Gabius, H.-J.; Percec, V. Glycodendrimersomes from sequence-defined Janus glycodendrimers reveal high activity and sensor capacity for the agglutination by natural variants of human lectins. *J. Am. Chem. Soc.* **2015**, *137*, 13334−13344.
(38) Xiao, Q.; Zhang, S.; Wang, Z.; Sherman, S. E.; Moussodia, R.-O.; Peterca, M.; Muncan, A.; Williams, D. R.; Hammer, D. A.; Vértesy, S.; André, S.; Gabius, H.-J.; Klein, M. L.; Percec, V. Onion-like glycodendrimersomes from sequence-defined Janus glycodendrimers and influence of architecture on reactivity to a lectin. *Proc. Natl. Acad. Sci. U. S. A.* **2016**, *113*, 1162−1167.
(39) Xiao, Q.; Yadavalli, S. S.; Zhang, S.; Sherman, S. E.; Fiorin, E.; da Silva, L.; Wilson, D. A.; Hammer, D. A.; André, S.; Gabius, H.-J.; Klein, M. L.; Goulian, M.; Percec, V. Bioactive cell-like hybrids coassembled from (glyco)dendrimersomes with bacterial membranes. *Proc. Natl. Acad. Sci. U. S. A.* **2016**, *113*, E1134−E1141.
(40) Peterca, M.; Percec, V.; Leowanawat, P.; Bertin, A. Predicting the size and properties of dendrimersomes from the lamellar structure of their amphiphilic Janus dendrimers. *J. Am. Chem. Soc.* **2011**, *133*, 20507−20520.
(41) Xiao, Q.; Rubien, J. D.; Wang, Z.; Reed, E. H.; Hammer, D. A.; Sahoo, D.; Heiney, P. A.; Yadavalli, S. S.; Goulian, M.; Wilner, S. E.; Baumgart, T.; Vinogradov, S. A.; Klein, M. L.; Percec, V. Self-sorting and coassembly of fluorinated, hydrogenated, and hybrid Janus dendrimers into dendrimersomes. *J. Am. Chem. Soc.* **2016**, *138*, 12655−12663.
(42) Zhang, S.; Moussodia, R.-O.; Murzeau, C.; Sun, H.-J.; Klein, M. L.; Vértesy, S.; André, S.; Roy, R.; Gabius, H.-J.; Percec, V. Dissecting molecular aspects of cell interactions using glycodendrimersomes with programmable glycan presentation and engineered human lectins. *Angew. Chem., Int. Ed.* **2015**, *54*, 4036−4040.
(43) Zhang, S.; Moussodia, R.-O.; Vértesy, S.; André, S.; Klein, M. L.; Gabius, H.-J.; Percec, V. Unraveling functional significance of natural variations of a human galectin by glycodendrimersomes with programmable glycan surface. *Proc. Natl. Acad. Sci. U. S. A.* **2015**, *112*, 5585−5590.
(44) Gabius, H.-J.; Kaltner, H.; Kopitz, J.; André, S. The glycobiology of the CD system: a dictionary for translating marker designations into glycan/lectin structure and function. *Trends Biochem. Sci.* **2015**, *40*, 360−376.
(45) Loris, R.; Hamelryck, T.; Bouckaert, J.; Wyns, L. Legume lectin structure. *Biochim. Biophys. Acta, Protein Struct. Mol. Enzymol.* **1998**, *1383*, 9−36.
(46) Meagher, J. L.; Winter, H. C.; Ezell, P.; Goldstein, I. J.; Stuckey, J. A. Crystal structure of banana lectin reveals a novel second sugar binding site. *Glycobiology* **2005**, *15*, 1033−1042.
(47) Singh, D. D.; Saikrishnan, K.; Kumar, P.; Surolia, A.; Sekar, K.; Vijayan, M. Unusual sugar specificity of banana lectin from *Musa paradisiaca* and its probable evolutionary origin. *Glycobiology* **2005**, *15*, 1025−1032.
(48) Swanson, M. D.; Boudreaux, D. M.; Salmon, L.; Chugh, J.; Winter, H. C.; Meagher, J. L.; André, S.; Murphy, P. V.; Oscarson, S.; Roy, R.; King, S.; Kaplan, M. H.; Goldstein, I. J.; Tarbet, E. B.; Hurst, B. L.; Smee, D. F.; de la Fuente, C.; Hoffmann, H.-H.; Xue, Y.; Rice, C. M.; Schols, D.; Garcia, J. V.; Stuckey, J. A.; Gabius, H.-J.; Al-Hashimi, H. M.; Markovitz, D. M. Engineering a therapeutic lectin by uncoupling mitogenicity from antiviral activity. *Cell* **2015**, *163*, 746−758.
(49) Swanson, M. D.; Winter, H. C.; Goldstein, I. J.; Markovitz, D. M. A lectin isolated from bananas is a potent inhibitor of HIV replication. *J. Biol. Chem.* **2010**, *285*, 8646−8655.
(50) Liu, F.-T.; Rabinovich, G. A. Galectins as modulators of tumour progression. *Nat. Rev. Cancer* **2005**, *5*, 29−41.
(51) Yang, R.-Y.; Rabinovich, G. A.; Liu, F.-T. Galectins: structure, function and therapeutic potential. *Expert Rev. Mol. Med.* **2008**, *10*, e17.
(52) Thurston, T. L. M.; Wandel, M. P.; von Muhlinen, N.; Foeglein, Á.; Randow, F. Galectin 8 targets damaged vesicles for autophagy to defend cells against bacterial invasion. *Nature* **2012**, *482*, 414−418.
(53) Bhat, R.; Belardi, B.; Mori, H.; Kuo, P.; Tam, A.; Hines, W. C.; Le, Q.-T.; Bertozzi, C. R.; Bissell, M. J. Nuclear repartitioning of galectin-1 by an extracellular glycan switch regulates mammary morphogenesis. *Proc. Natl. Acad. Sci. U. S. A.* **2016**, *113*, E4820−E4827.
(54) Sagalowicz, L.; Acquistapace, S.; Watzke, H. J.; Michel, M. Study of liquid crystal space groups using controlled tilting with cryogenic transmission electron microscopy. *Langmuir* **2007**, *23*, 12003−12009.
(55) Davis, K. P.; Lodge, T. P.; Bates, F. S. Vesicle membrane thickness in aqueous dispersions of block copolymer blends. *Macromolecules* **2008**, *41*, 8289−8291.
(56) Demurtas, D.; Guichard, P.; Martiel, I.; Mezzenga, R.; Hébert, C.; Sagalowicz, L. Direct visualization of dispersed lipid bicontinuous cubic phases by cryo-electron tomography. *Nat. Commun.* **2015**, *6*, 8915.
(57) Cairo, C. W.; Gestwicki, J. E.; Kanai, M.; Kiessling, L. L. Control of multivalent interactions by binding epitope density. *J. Am. Chem. Soc.* **2002**, *124*, 1615−1619.
(58) Blouin, C. M.; Hamon, Y.; Gonnord, P.; Boularan, C.; Kagan, J.; Viaris de Lesegno, C.; Ruez, R.; Mailfert, S.; Bertaux, N.; Loew, D.; Wunder, C.; Johannes, L.; Vogt, G.; Contreras, F.-X.; Marguet, D.; Casanova, J.-L.; Galès, C.; He, H.-T.; Lamaze, C. Glycosylation-dependent IFN-γR partitioning in lipid and actin nanodomains is critical for JAK activation. *Cell* **2016**, *166*, 920−934.
(59) Norlén, L. Skin barrier formation: the membrane folding model. *J. Invest. Dermatol.* **2001**, *117*, 823−829.
(60) Kremer, J. R.; Mastronarde, D. N.; McIntosh, J. R. Computer visualization of three-dimensional image data using IMOD. *J. Struct. Biol.* **1996**, *116*, 71−76.

DOI: 10.1021/acscentsci.6b00284
ACS Cent. Sci. 2016, 2, 943−953